Supplementary Information

Enhanced charge transport and photovoltaic performance induced by incorporating rare-earth phosphor in organic/inorganic hybrid solar cells

Zihan Chen[1,§], Qinghua Li[1,§,*], Chuyang Chen[2], Jiaxing Du[3], Jifeng Tong[3], Xiao Jin[1], Yue Li[1], Yongbiao Yuan[1], Yuancheng Qin[1], Taihuei Wei[4,*], Weifu Sun[2,*]

[1]Key Laboratory of Nondestructive Testing，Ministry of Education, Nanchang Hangkong University, Nanchang, 330063, P. R. China

[2]School of Materials Science and Engineering, The University of New South Wales, Sydney, NSW 2052, Australia

[3]Institute of the Ministry of Science Research, Academy of Armored Force Engineering, Beijing, 100072, P. R. China

[4]Department of Physics, National Chung-Cheng University, Chia-Yi 621, Taiwan, Republic of China

*Corresponding author: E-mail address: qhli@hqu.edu.cn, Tel.: +86 791 8645 3203, Fax: +86 791 8645 3203; twei@ccu.edu.tw; weifu.sun518@gmail.com.

§These authors contributed equally.

1. Photoluminescence and optimal initial loading of Dy^{3+}

The excitation spectrum with $\lambda_{emission}$ =575 nm is shown in Figure S1 (black line). The excitation spectrum consists of three parts: a broad band from 315 to 341 nm with the weak intensity attributed to the absorption of the Dy^{3+}:Y_2O_3 host lattice; the strong excitation peak at 375 nm that is assigned to the electronic transitions of Dy^{3+} ion from the ground state $^6H_{15/2}$ to the excited level $^6P_{1/2}$; the red line that shows the photoluminescence spectra of the Dy^{3+}:Y_2O_3 film under 375-nm excitation. A main peak locates at 575 nm, corresponding to the transitions of Dy^{3+} ions: $^4F_{9/2} \rightarrow {}^6H_{13/2}$ [1].

A weak peak at 486 nm is attributed to the transitions $^6P_{1/2} \rightarrow {}^6H_{11/2}$. Note that these luminescence bands are located in the absorption range of the P3HT. Combining the excitation and emission spectra, the ultraviolet irradiation can be absorbed by P3HT via down-conversion luminescence, which widens the light absorption range of the HSCs.

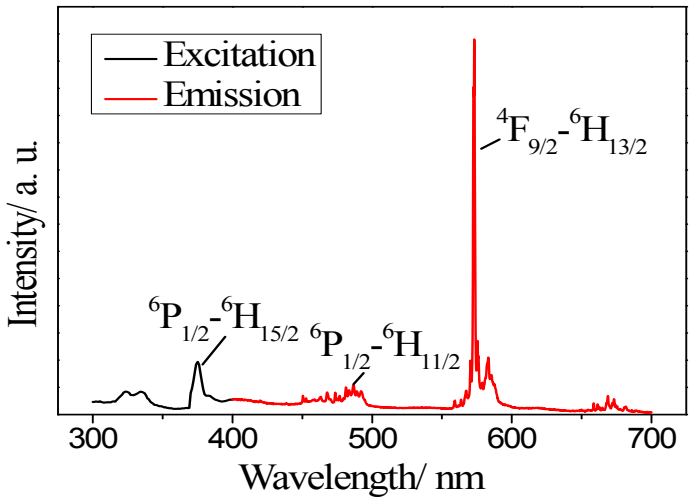

Figure S1. Photoluminescence spectra of Dy^{3+}:Y_2O_3 film: excitation (black line), emission (red line).

The optimal initial loading of Dy^{3+} relative to Y_2O_3 was studied using the incident photon-to-current conversion efficiency (IPCE) measurement. In order to investigate influence of the doping amounts of Dy^{3+} on the performance of the solar cells, different initial molar loading of Dy^{3+} relative to Y_2O_3 was used and the incident photon-to-current conversion efficiency (IPCE) measurements were performed and the results are shown in Figure S2, whereas the loading amounts of Yittrium species was kept unchanged.

First, a notable increase of IPCE around 400 nm can be observed when the

contents of Dy^{3+} increases from 1% to 5% (mole ratio of Dy^{3+} relative to Y_2O_3), and this can be attributed to the enhancement of down-conversion process stemming from Dy^{3+}. The down-conversion process converts the solar spectrum near 400 nm to 500~600 nm visible range (detailed analysis are shown in Supporting Information Figure S1), thus light harvest can be better absorbed by P3HT molecules and a notable increase in IPCE around 375 nm was achieved. However, to our surprise, with further adding of Dy^{3+} up to 7%, the IPCE decreases. This decrease may be ascribed to the quenching of the luminescence that arises from the introducing of deleterious cross-relaxation by elevated doping levels (F. Wang, et al., Nat. Mater., 2011, 10, 968-973). Therefore, when the initial loading of Dy^{3+} is about 0.002 mol in this work, the device exhibits the best performances. Meanwhile, the broad IPCE curves covering the spectrum from 450 to 600 nm are almost independent of the contents of Dy^{3+}, exhibiting a maximum IPCE value of about 47%, and this is consistent with the UV-vis spectrum of P3HT as shown in Figure S3.

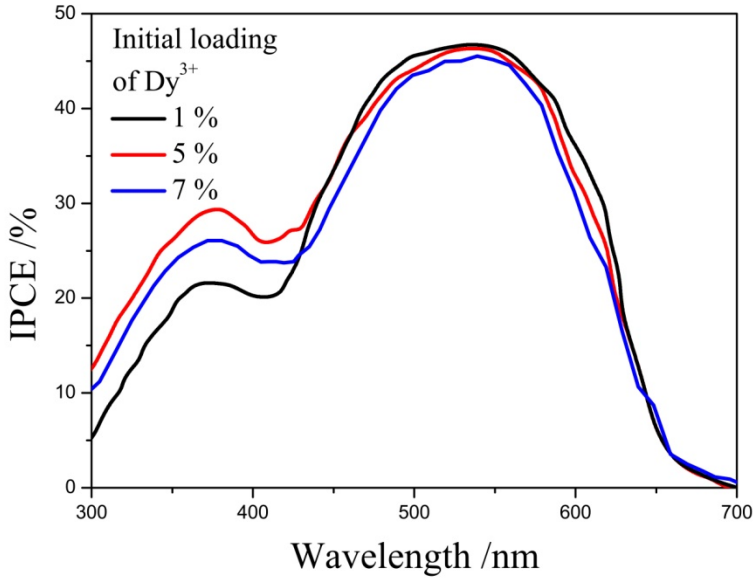

Fig. S2 IPCE of Dy^{3+}:Y_2O_3-TiO2/P3HT solar cells with different initial loading

amounts of Dy^{3+} (molar ratio of Dy^{3+} relative to Y_2O_3).

2. Energy level engineering

In order to enhance efficiency even further, research activities are needed in pursuit of new materials with better aligned energy levels. In HSCs, the conduction band (CB) edge location is as important as the band gap of the semiconductor, because the position of the CB edge should always be located lower than the LUMO level of the donor. The energy level difference between donor and acceptor would play an important role in the charge transfer from donor to bulk-heterojunction interface. The energy levels of the donor and acceptor are critical to ensure an efficient photogenerated charge transfer. In order to investigate the energy level regulation of acceptor induced by Dy^{3+} doping, cyclic voltammetry (CV) is a dynamic electrochemical method, in which current-potential curves are recorded at well-defined applied potential [2,3]. Cyclic voltammetric characteristics were performed within an electrochemical inert gas cell inside a Faraday cage. The cell was purged with pure argon prior to each scan. The scans toward the anodic and cathodic directions were performed at a scan rate of 50mV/s at room temperature. The ferrocene ($E_{1/2}$ vs Ag/Ag^+ =0.09 eV) potential as a standard should be measured in the electrolyte solution using the same reference electrode, and -4.80 eV fixed as an energy level in the vacuum set. Finally the energy levels of HOMO and LUMO can be calculated using the following formula: HOMO (or LUMO) (eV)=-4.8-(E_{onset}-$E_{1/2}$), where E_{onset} is a starting point of the redox potential[4]. Electrochemical p- and n-doping properties of the three films (Dy^{3+}:Y_2O_3, Dy^{3+}:Y_2O_3-TiO_2, TiO_2) were studied,

respectively, by cyclic voltammetry.

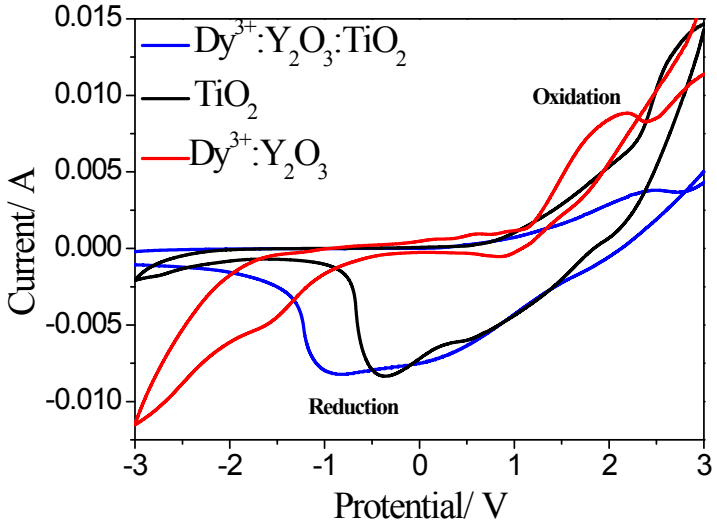

Figure S3. The CV behavior of the TiO_2, Dy^{3+}:Y_2O_3 and Dy^{3+}:Y_2O_3-TiO_2 electrodes in acetonitrile containing 0.1 M $TBAPF_6$ at a sweep rate of 50 mV/s.

The oxidation and reduction of the semiconductor nanocrystals films are shown in Figure S3, and all the electrochemical redox data are summarized in Table S1. Both oxidation and reduction waves are clearly revealed in the CV curves, implying that these semiconductor nanocrystals have the capability to transport both electrons and holes. On sweeping the films cathodically, the onset potentials of the pure TiO_2, Dy^{3+}:Y_2O_3 and Dy^{3+}:Y_2O_3-TiO_2 thin films occured at about -0.38, -1.56, -0.95 V, respectively and thus the LUMO energy levels of the corresponding films were estimated to be -4.33, -3.15, -3.76 eV, respectively. On anodic sweep, the onset potentials of TiO_2, Dy^{3+}:Y_2O_3 and Dy^{3+}:Y_2O_3-TiO_2 were determined to be 2.65, 2.09, and 2.33 V, corresponding to an HOMO energy level of -7.36, -6.80, and -7.04 eV, respectively. These results indicate that both the LUMO and HOMO energy levels of these films could be affected by the doping of Dy^{3+}: the HOMO of Dy^{3+}:Y_2O_3 doped TiO_2 is distinctively higher y than that of TiO_2 while the LUMO of Dy^{3+}:Y_2O_3-TiO_2 is

distinctively lower than that of TiO_2. Moreover, when doping with Dy^{3+}, it will give a doping effect, which results in the elevation of Fermi level of TiO_2 electrode (more negative to the vacuum level) and an increase of the V_{oc} values [5].

We use either the pure TiO_2 or Dy^{3+}:Y_2O_3 doped TiO_2 as charge-acceptor and P3HT charge-donor materials, respectively. The absorption spectrum of P3HT is shown in Figure S4(a). Note that the absorption spectra of P3HT exhibit two absorption maxima at 602 and 480 nm. Photoluminescence (PL) emission spectra of pure TiO_2/P3HT and Dy^{3+}:Y_2O_3 doped TiO_2 bulk-heterojunction excited at 602 nm are shown in Figure S4(b). In Dy^{3+}:Y_2O_3-TiO_2/P3HT film a stable and strong ultraviolet emission band centered at 381 nm is observed, which is attributed to the fluorescence of Dy^{3+}:Y_2O_3-TiO_2. The shoulder at 384 nm is attributed to the recombination of electrons and holes across the band edge and acceptor levels related to interstitial acceptor and donor levels due to native defects in the Dy^{3+}:Y_2O_3-TiO_2 lattices respectively. Under the excitation of 602-nm radiations, the P3HT molecules electrons are promoted to the conduction bands. These excited electrons then inject into conduction bands of Dy^{3+}:Y_2O_3-TiO_2, and then the electrons inevitably relax to the valence bands to induce the fluorescence. Therefore, the band gap of Dy^{3+}:Y_2O_3-TiO_2 can be estimated to be 3.24 eV [6]. Similarly, in pure TiO_2/P3HT, the strong violet emission band centered at 401 nm which correspond to a band gap of 3.09 eV. The results are consistent with those obtained from CV characterization results.

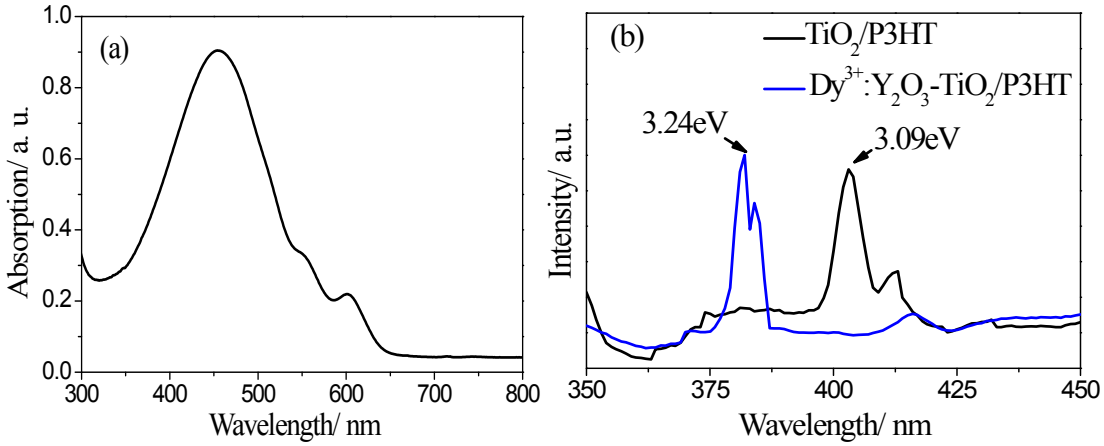

Figure S4. (a) The UV-vis absorption spectra of P3HT. (b) Photoemission spectra of Dy^{3+}:Y_2O_3-TiO_2 /P3HT and TiO_2/P3HT bulk-heterojunction excited at 602 nm.

Table S1. Electrochemical and photoluminescence data of the films.

Films	E^{red}_{onset} (V) /LUMO(eV)	E^{ox}_{onset} (V) /HOMO(eV)	E_g^a (eV)	λ^{P3HT} (nm) E xcitation	λ^{film}_{max} (nm) E mission	E_g^b (eV)
TiO_2	-0.38/-4.33	2.65/-7.36	3.03	602	401	3.09
Dy^{3+}:Y_2O_3	-1.56/-3.15	2.09/-6.80	3.65			
Dy^{3+}:Y_2O_3-TiO_2	-0.95/-3.76	2.33/-7.04	3.28	602	381	3.24

[a]Electrochemical band gap was calculated from the LUMO and HOMO energy levels.

[b]Optical band gap was estimated from the wavelength of the photoluminescence of the films.

Mott–Schottky plots (C^{-2} vs. V) are a standard means for the electrochemical characterization of semiconductor materials. For the n-type semiconductor, the relationship between the capacitance (C) and the applied potential (V) can be expressed by using Equation (S-1):

$$C^{-2} = \frac{2}{A^2 \varepsilon \varepsilon_0 N_D}\left(V - V_{FB} - \frac{kT}{e}\right) \quad \text{(S1)}$$

in which N_D is the doping density, V_{FB} is the flat-band (FB) potential, k is the Boltzmann constant, T is the temperature, ε is the relative dielectric constant of the anodic film, ε_0 is the permittivity of free space, e is the charge of an electron, and A is the electrode area. The flat band potentials were determined by Mott-Schottky plots as obtained by a linear extrapolation to C=0, *i.e.*, the intercept at the X axis.[7] Then, the conduction band (CB) energy level was calculated with Ag/Ag^+ as reference. Finally, the valence band (CB) energy level was obtained and listed in Table S2. As observed from Table S2, for given doping concentration at 6 wt%, the CB values obtained from the CV characteristics are in reasonable agreement with those determined from Mott-Schottky method, indicating that the results obtained in this work are reliable.

Table S2. Electrochemical data of the films obtained from Mott-Schottky plots.

Loading amounts of Dy^{3+}:Y_2O_3 (wt%)	0	2	4	6	8
FB potential (V)/CB[b] (eV)	-0.52/-4.19	-0.62/-4.09	-0.80/-3.91	-0.94/-3.77	-0.99/-3.72

3. The transient absorption spectrum of BHJ

Fig. S5 shows the representative transient absorption spectra of donor/acceptor films measured from 1 to 900 ps. Note that both the negative and the positive peaks decay quickly from 0 to 30 ps, indicating that there exist fast mechanisms influencing PB and PA. However, on the longer time scale (30 to 900 ps), PA peaks decay slowly whereas the PB peaks increase slightly although not so obviously. The difference characteristics of PA and PB signals are attributed to complex electronic contributions

such as charge generation, transfer, and recombination. Accordingly, the transient absorption data we observed may be taken as a convolution of the background-free laser pulse autocorrelation function G(t) with the response function [8,9].

$$S(\tau) = \int_{-\infty}^{+\infty} G(\tau - t)\phi(\mathrm{t})\,\mathrm{d}\,t \tag{S2}$$

The response function ϕ(t) may be taken to be a linear superposition of electronic contributions.

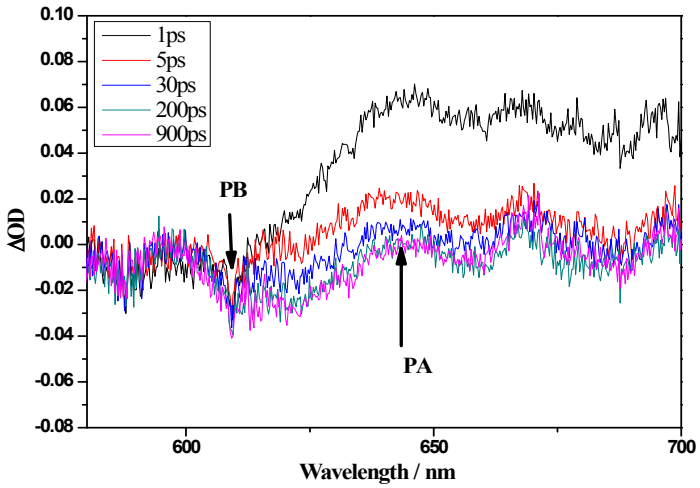

Figure S5. Differential absorption spectra for Dy^{3+}:Y_2O_3-TiO_2/P3HT film after excitation at 400nm: black (1 ps), red (5 ps), blue (30 ps), green (200 ps), pink (900 ps).

4. Open circuit voltage

According to the following relationship [10],

$$V_{\mathrm{OC}} = \left|\mathrm{HOMO_D}\right| - \left|\mathrm{LUMO_A}\right| - \frac{kT}{q}\ln\left(\frac{N_{eff}^2}{np}\right) \tag{S3}$$

where $\mathrm{HOMO_D}$ is the highest occupied molecular orbital (HOMO) of the donor, $\mathrm{LUMO_A}$ is the LUMO of the acceptor, k is the Boltzmann constant, q is the elementary charge, T is temperature, N_{eff} is the effective density of state, and n and p

are the concentrations of electrons and holes, respectively. If the third term is neglected, V_{oc} is determined by the energy-level difference between the $|HOMO_D|$ and $|LUMO_A|$. One route to improve V_{oc} is to raise the CB energy level of the acceptor (*i.e.*, to decrease $|LUMO_A|$), which will simultaneously reduce the energy offset between the CB energy level of acceptor and LUMO energy level of donor.

5. Time-integrated PL

Time-integrated PL measurements were provided to identify the charge transfer properties with selected electron/hole-only extraction layer, as shown in Figure S6. It is known that the PL spectrum of P3HT is sensitive to the degree of the photoinduced charge transfer to the acceptor. Compared to TiO_2/P3HT, an efficient PL quenching for Dy^{3+}:Y_2O_3 -TiO_2/P3HT blend film can be ascribed to the redundant space provided or pores formed by the incorporation of Dy^{3+}:Y_2O_3 nanoparticles, thus favoring the physical adsorptions of P3HT molecules and forming intimate contact between P3HT molecules and acceptor. After incorporating Dy^{3+}:Y_2O_3 nanoparticles into TiO_2, the interface contact between donor and acceptor has been improved, thus benefiting efficient charge transfer in BHJ. Besides, as for the hole-only device P3HT/PEDOT:PSS, the emission intensity of P3HT was quenched intensely after coating on the hole extraction layer PEDOT:PSS. These high degrees of PL quenching indicate that the current configuration of Dy^{3+}:Y_2O_3 -TiO_2/P3HT bears good electron and hole transport properties.

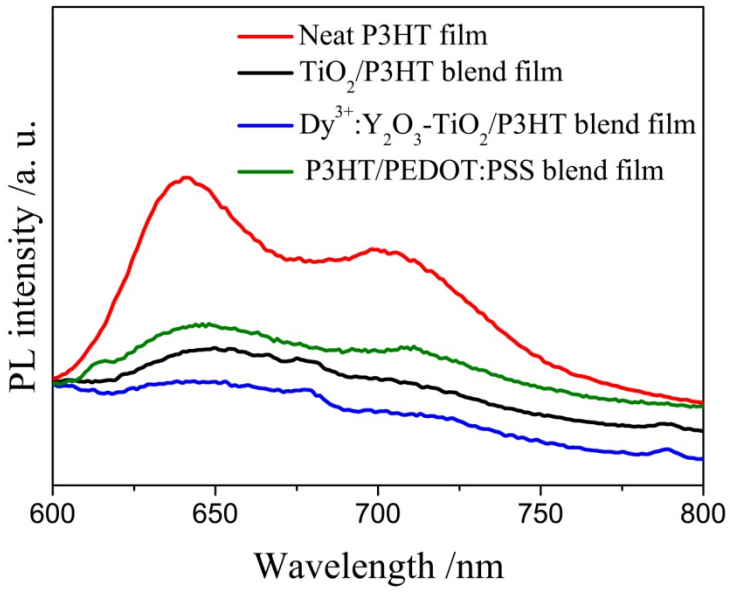

Figure S6. Steady state PL for neat P3HT, TiO_2/P3HT, Dy^{3+}:Y_2O_3-TiO_2/P3HT, P3HT/PEDOT:PSS blend films.

Supplementary references

1 F. Wang, R. Deng, J. Wang, Q. Wang, Y. Han, H. Zhu, X. Chen and X. Liu, *Nat. Mater.*, **2011**, *10*, 968-973.

2 J.-S. Wu, Y.-J. Cheng, T.-Y. Lin, C.-Y. Chang, P.-I. Shih and C.-S. Hsu, *Adv. Funct. Mater.*, **2012**, *22*, 1711-1722.

3 Q. Peng, X. Liu, D. Su, G. Fu, J. Xu and L. Dai, *Adv. Mater.*, **2011**, *23*, 4554-4558.

4 Y. Li, H. Zhong, R. Li, Y. Zhou, C. Yang and Y. Li, *Adv. Funct. Mater.*, **2006**, *16*, 1705-1716.

5 M. Grätzel, *Nature*, **2001**, *414*, 338-344.

6 E. A. Axtell, J. H. Liao, Z. Pikramenou and M. G. Kanatzidis, *Chem.-A Eur. J.*, **1996**, *2*, 656-666.

7 J. L. Wang, J. H. Wu, J. M. Lin, M. L. Huang, Y. F. Huang, Z. Lan, Y. M.

Xiao, G. T. Yue, S. Yin and T. Sato, *ChemSusChem*, **2012**, *5*, 1307-1312.

8 D. McMorrow, W. T. Lotshaw and G. A. Kenney-Wallace, *IEEE J. Quantum Elect.*, **1988**, *24*, 443-454.

9 D. McMorrow and W. T. Lotshaw, *J. Phys. Chem.*, **1991**, *95*, 10395-10406.

10 R. Kroon, M. Lenes, J. C. Hummelen, P. W. M. Blom and B. de Boer, *Polym. Rev.*, **2008**, *48*, 531-582.